Cryogenic Performance of Double-Fused 1.5-μm Vertical Cavity Lasers

Y. M. Zhang, J. Piprek, *Senior Member, IEEE,* N. Margalit, M. Anzlowar, and J. Bowers, *Fellow, IEEE*

***Abstract*—The low-temperature performance of vertical cavity lasers (VCL's) is of interest for high-speed data transmission from superconducting and cryogenic semiconductor circuits. Our double-fused 1.5 μm lasers employ a strain-compensated InGaAsP/InP multiquantum-well (MQW) active region that is sandwiched between two AlGaAs/GaAs distributed Bragg reflectors. Continuous wave (CW) lasing at ambient temperature as low as 7 K is measured on the same type of top-emitting devices that previously lased at a record-high temperature of 337 K. The optimum temperature is found at 180 K giving minimum threshold current, maximum modulation bandwidth of 5 GHz, and more than 3 GHz/mA$^{1/2}$ modulation current efficiency. The optimum temperature agrees very well with the theoretical prediction. Further device optimization for cryogenic high-speed applications is discussed in detail.**

***Index Terms*— Cryogenic electronics, microwave modulation, optical fiber communication, semiconductor lasers, surface-emitting lasers, wavelength measurement.**

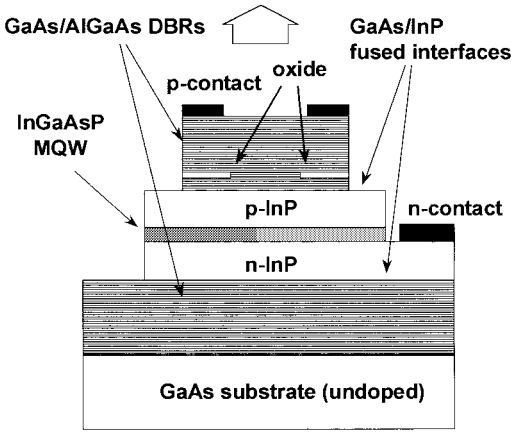

Fig. 1. Schematic drawing out of top-emitting double-fused 1.5 μm vertical cavity laser with lateral oxidation of the top mirror.

I. Introduction

LOW-THRESHOLD cryogenic vertical cavity lasers (VCL's) are of interest for high-speed optical links based on superconducting electronics or other low-voltage level cryogenic semiconductor electronics (such as cryo-complementary metal–oxide–semicoductor (CMOS) circuits). Possible applications of such optical links are in space satellite communications where driver circuitry and power dissipation must be kept at an absolute minimum. Low-threshold VCL's are also of interest for terabit/s optical transmission systems that require many laser transmitters (e.g., 200 VCL's, at 5 Gbit/s each) for the huge data transfer in high energy and nuclear physics, as well as in future petaflops-scale computing networks. In general, semiconductor lasers are expected to offer superior performance at low temperatures as a result of higher gain (both absolute and differential), lower loss, and higher quantum efficiency. Performance improvements include smaller threshold current, higher modulation bandwidth, and higher power conversion efficiency. Compared to in-plane lasers, VCL advantages include small active volume, low power dissipation, compact packaging, and low cost. Cryogenic short-wavelength VCL technology (below 1 μm emission wavelength) is well developed [1]. Submilliamp threshold current (120 μA) has been demonstrated at 77 K for an optimized 950 nm VCL [2]. However, short-wavelength VCL's are only suitable for short-haul data communication due to high fiber loss, wavelength dispersion, and lack of optical amplifiers. Long-wavelength VCL's (1.3 and 1.55 μm) are the desired low cost sources for long-haul fiber optical communication.

The best performance of 1.55 μm VCL's has been achieved utilizing InP/GaAs wafer fusion [3], [4]. These double-fused lasers employ a strain-compensated InGaAsP/InP multiquantum-well (MQW) active region that is sandwiched between two AlGaAs/GaAs distributed Bragg reflectors (DBR's). Lateral oxidation is applied to the top p-doped DBR pillar of the device for confinement of current and optical mode. The lasers used here are top-emitting with an intracavity n-contact and an undoped bottom DBR (Fig. 1). More details on the devices are given in [4]. These double-fused VCL's exhibit continuous wave (CW) operation up to a record-high ambient temperature of 64 °C (with a 6-μm oxide aperture). In this paper, we present detailed results on their cryogenic performance. All devices investigated have about a 12-μm oxide aperture in order to obtain higher output power. The temperature dependence of emission wavelength, threshold current, slope efficiency, and threshold voltage as well as the current modulation response are investigated for stage temperatures between 7–291 K.

II. Theory

Lowering the operating temperature strongly affects the MQW optical gain. Fig. 2 shows gain spectra at different MQW temperatures as calculated using a 4 $\times$ 4 kp band

Manuscript received August 4, 1998; revised October 29, 1998. This work was supported in part by DOE SBIR Grant DE-FG03-97ER82355.

Y. M. Zhang is with Conductus, Inc., Sunnyvale, CA 94086 USA.

J. Piprek, N. Margalit, M. Anzlowar, and J. Bowers are with the Electrical and Computer Engineering Department, University of California, Santa Barbara, CA 93106 USA.

Publisher Item Identifier S 0733-8724(99)01900-3.

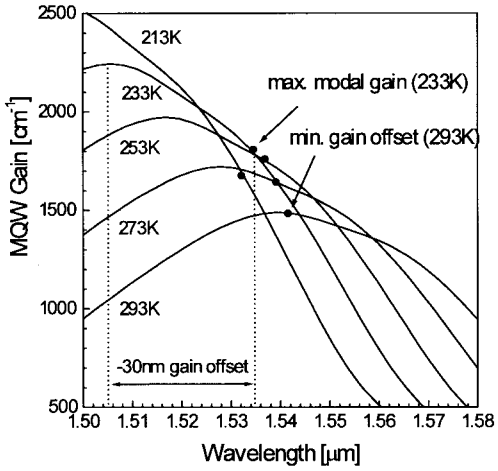

Fig. 2. Calculated MQW gain spectra at different temperatures (lines). The dots give the VCL emission wavelength at each temperature and they indicate the modal gain.

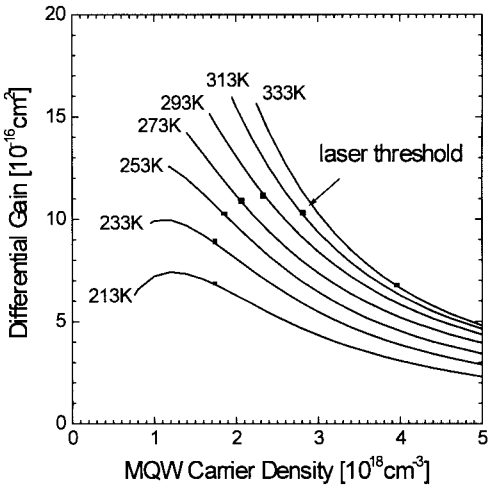

Fig. 3. Calculated differential gain as function of carrier density and temperature. The dots indicate the lasing threshold. The starting point of each curve gives the transparency density.

structure and Fermi's Golden rule (including many body effects). As the temperature is reduced, the peak gain increases but its wavelength λ_{gain} also moves toward smaller values. This blue-shift $\lambda_{\text{gain}}(T)$ is due to the temperature dependence of the electron energy band gap. The increase of the gain peak is caused by a steeper Fermi distribution function of electrons. In edge-emitting Fabry–Perot lasers, the emission wavelength follows the gain peak, and light amplification increases at lower temperatures resulting in a monotonically decreasing threshold current [5]. This situation is different in VCL's and other lasers with stabilized emission wavelength. The short vertical length of the VCL cavity results in a single longitudinal optical mode at an emission wavelength λ_{cav} which is given by the optical distance of the distributed Bragg reflectors. The wavelength $\lambda_{\text{cav}}(T)$ blue-shifts with lower temperature due to the refractive index change. But this shift is much slower than the shift of the gain peak $\lambda_{\text{gain}}(T)$. The dots in Fig. 2 indicate $\lambda_{\text{cav}}(T)$ and show the modal gain at each temperature. We notice that the maximum modal gain is obtained at an optimum temperature $T_{\text{opt}} = 233\,\text{K}$ which is about 60 K below the temperature 293 K for zero gain offset ($\lambda_{\text{gain}} = \lambda_{\text{cav}}$). The optimum gain offset $\lambda_{\text{gain}} - \lambda_{\text{cav}}$ is found to be dependent on the MQW material and it is about -30 nm for our InGaAsP/InP MQW's [6]. The temperature dependence of the VCL modal gain results in a minimum of the threshold current $I_{\text{th}}(T)$ near $T = T_{\text{opt}}$. MQW loss mechanisms like Auger recombination and intervalence band absorption also affect the $I_{\text{th}}(T)$ minimum but they are considered to be less important at low temperatures [6]. Additional temperature effects might originate from thermionic emission at the fused interface and from changes of the carrier mobility.

The actual value of T_{opt} depends on the specific VCL design. The gain peak wavelength shift

$$\lambda_{\text{gain}}(T) = \lambda_{\text{gain}}(300\ \text{K}) + \beta_{\text{gain}} \cdot (T - 300\ \text{K}) \qquad (1)$$

is affected by the MQW design. Measurements on strain-compensated 1.55 μm MQW's similar to ours give the temperature coefficient $\beta_{\text{gain}} = 0.54$ nm/K [7]. The emission wavelength

$$\lambda_{\text{cav}}(T) = \lambda_{\text{cav}}(300\ \text{K}) + \beta_{\text{cav}} \cdot (T - 300\ \text{K}) \qquad (2)$$

may also vary from wafer to wafer; its temperature coefficient β_{cav} is on the order of 0.1 nm/K. At the optimum operating temperature T_{opt}, $\lambda_{\text{cav}}(T) = \lambda_{\text{gain}}(T)$. Changing the thickness of the InP spacer layer is a convenient method to modify λ_{cav} (300 K) and thereby change the optimum temperature. A lower T_{opt} can be achieved with a smaller emission wavelength λ_{cav} (300 K) or a larger gain peak wavelength λ_{gain} (300 K) (reduced MQW band gap). With our VCL's, the minimum pulsed threshold current $I_{\text{th}}(T_{\text{opt}})$ is expected at

$$\lambda_{\text{cav}}(T_{\text{opt}}) = \lambda_{\text{gain}}(T_{\text{opt}}) + 30\ \text{nm}. \qquad (3)$$

The analog modulation response also depends on the temperature. With constant dc current I, the resonance frequency f_r is mainly governed by the change of the threshold current $I_{\text{th}}(T)$,

$$f_r = \frac{\eta_m}{1.55}\sqrt{I - I_{\text{th}}} \qquad (4a)$$

$$\eta_m = \frac{1.55}{2\pi}\sqrt{\frac{dg}{dN}\frac{\Gamma v_g \eta_i}{qV}}\,. \qquad (4b)$$

Here η_m is the modulation current efficiency, dg/dN the differential gain, Γ the confinement factor, v_g the photon group velocity, η_i the internal quantum efficiency, q the electron charge, and V the active volume. The factor 1.55 relates to the bandwidth $f_{3\,\text{dB}} = 1.55 f_r$. The efficiency η_m varies with temperature. First of all, the differential gain dg/dN depends on temperature and carrier density N. Fig. 3 illustrates this dependence using the same gain model as in Fig. 2. The dots indicate the threshold carrier density $N_{\text{th}}(T)$ and give the corresponding differential gain as function of the ambient temperature. The maximum is reached at the smallest gain offset (293 K). The internal efficiency h_i may also decrease with lower temperature due to enhanced lateral current spreading.

III. Measurement Setup

The double-fused VCL chip is mounted onto a high-speed package with a gold ribbon between the K-connector launch center pin and the VCL p-side contact pad. The laser package sits on the cold plate of an Infrared Lab's two-stage cryogenic dewar that can be cooled by liquid nitrogen or liquid helium. A Lakeshore thermometer diode and a heater are attached to the cold plate near the laser package for temperature control. A semirigid coaxial cable is connected to the chip for dc bias and high-frequency microwave signal modulation. A 0.15 pitch graded-index (GRIN) rod lens in front of the laser collimates the light beam. The GRIN lens was adjusted at room temperature with a mini three-axis positioner (inside the dewar) to ensure maximum light output from the VCL through the antireflection-coated optical window of the dewar.

For light power output versus injection current (L–I) measurements, the light is coupled directly to a Newport near-infrared detector that is placed at room temperature near the optical window. For wavelength and modulation bandwidth measurements, the output light beam was collimated into a fiber using a Newport fiber positioner and an objective lens. For the emission wavelength measurement, the laser output light is coupled into an HP optical spectrum analyzer through a multimode fiber. For current modulation measurements, the RF input signal from an HP network analyzer is coupled to the cryogenic VCL through a wideband bias-tee, and the output light is coupled to a Lasertron 12-GHz photodetector at room temperature through a single-mode fiber. The optical alignment for coupling the laser beam into the single-mode fiber core was optimized at room temperature. Both CW and pulsed measurements (100 kHz at 1% duty-cycle) have been performed on these devices.

IV. Experimental Results

We measured the emission wavelength at different stage temperatures in pulsed laser operation to avoid self-heating. Fig. 4(a) shows the cavity emission wavelength $\lambda_{\rm cav}(T)$ between 130–260 K (the pulsed signal was very weak at lower temperatures). A transition between two modes (with about 1.8 nm wavelength difference) is observed with single mode operation below 180 K and above 220 K. The reason for the mode transition is unclear. The pulsed emission wavelength shows a linear blue shift of $\beta_{cav} = 0.08$ nm/K with decreasing temperature. This is mainly attributed to refractive index changes. Before fusion, we also measured the peak wavelength of the photoluminescence spectrum which is only a few nanometers shorter than the gain peak resulting in $\lambda_{\rm gain}\ (300\ {\rm K}) = 1540$ nm for our lasers.

Using (2), (3), and $\beta_{\rm gain} = 0.54$ nm/K [7], we plot $\lambda_{\rm gain}(T)$ and $\lambda_{\rm gain}(T)+30$ in Fig. 4(b). The measured emission wavelength $\lambda_{\rm cav}(T)$ is also plotted in the figure. In our case, perfect alignment of gain peak and emission wavelength is obtained near 250 K. But the minimum threshold current is expected at -30 nm gain offset, i.e., near 180 K. This optimum temperature is lower than the optimum temperature 233 K in Fig. 2 since our room-temperature emission wavelength

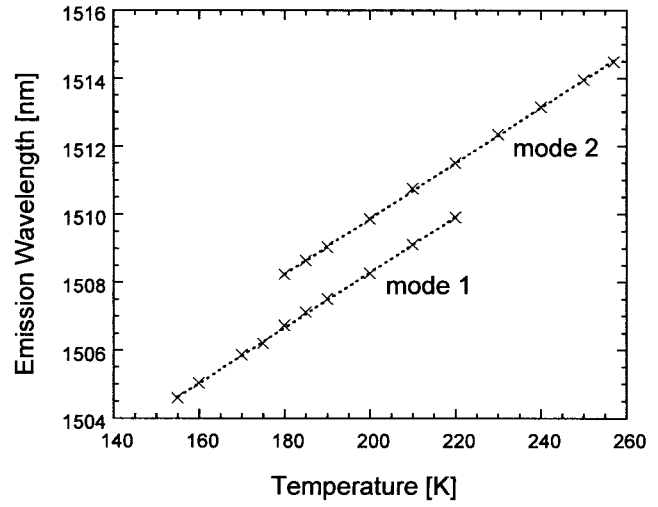

(a)

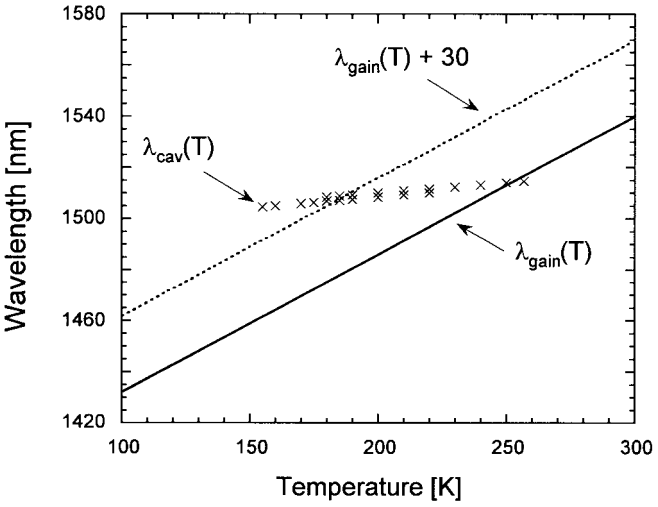

(b)

Fig. 4. (a) Measured emission wavelength $\lambda_{\rm cav}(T)$ versus temperature in pulsed operation at 16 mA current. Mode 1 dominates below 180 K, and mode 2 dominates above 180 K. (b) Comparison of measured $\lambda_{\rm cav}(T)$ (crosses) and calculated gain peak shift $\lambda_{\rm gain}(T)$ (solid line). The dashed line represents -30 nm gain offset and its crossover with $\lambda_{\rm cav}(T)$ gives the optimum temperature (180 K).

$\lambda_{\rm cav}\ (300\ {\rm K}) = 1518$ nm is somewhat smaller than the usual 1550 nm.

The measured pulsed threshold current $I_{\rm th}(T)$ and the threshold voltage $V_{\rm th}(T)$ are shown in Fig. 5. The optimum temperature $T_{\rm opt} = 180$ K agrees perfectly with our prediction from Fig. 4. This agreement confirms that the dominating influence comes from the optical gain. CW L–I characteristics of the VCL device are measured between room temperature and 7 K. They are given in Fig. 6 for temperatures below 180 K, showing a strong increase of the threshold current $I_{\rm th}$ with decreasing temperature. The measured output power is well below 1 mW and the wall-plug efficiency is less than 1%. This is partially due to misalignment losses between the low-temperature laser and the room-temperature detector. We calculate the slope efficiency from the L–I curves. The maximum slope efficiency is about 50 mW/A at 180 K. With decreasing temperature, the slope efficiency is reduced. But at

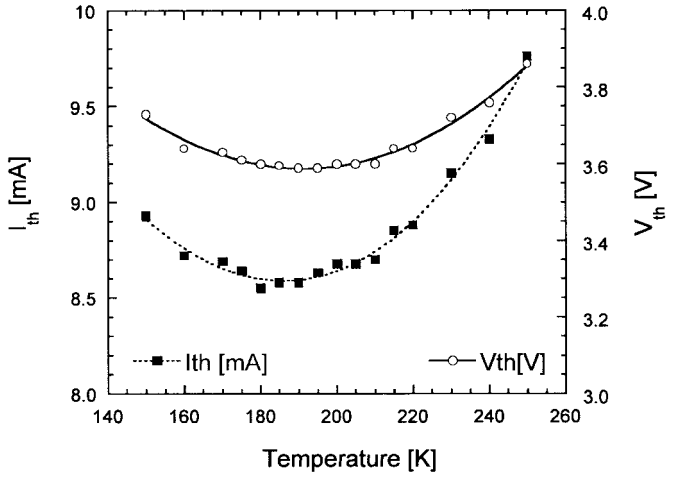

Fig. 5. Measured pulsed threshold current and threshold voltage versus ambient temperature.

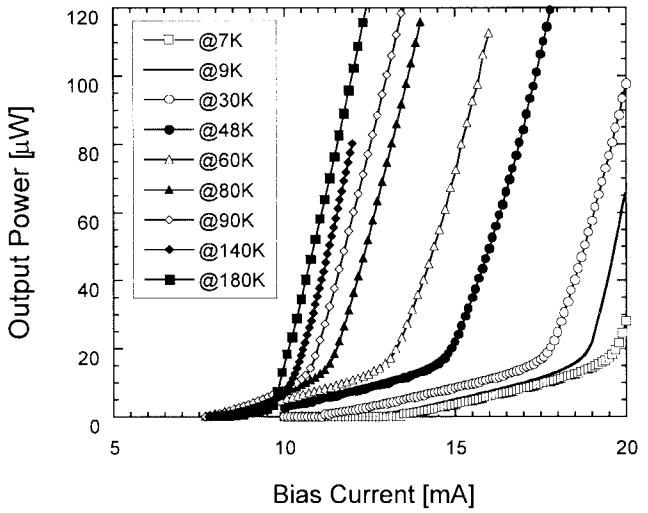

Fig. 6. Coupled optical output power versus injected CW current (L–I) measured at different temperatures below 180 K.

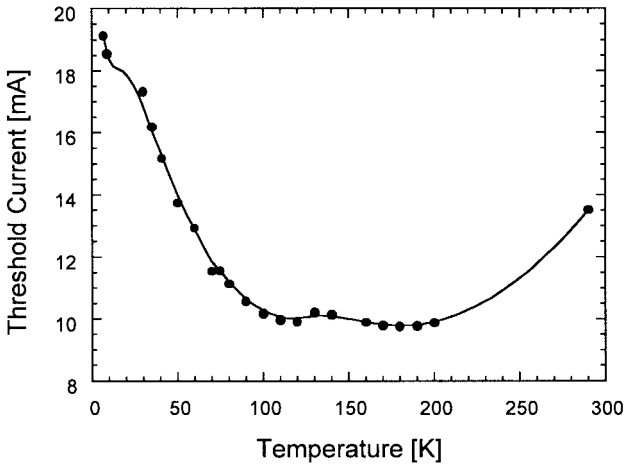

Fig. 7. Measured CW threshold current versus ambient temperature.

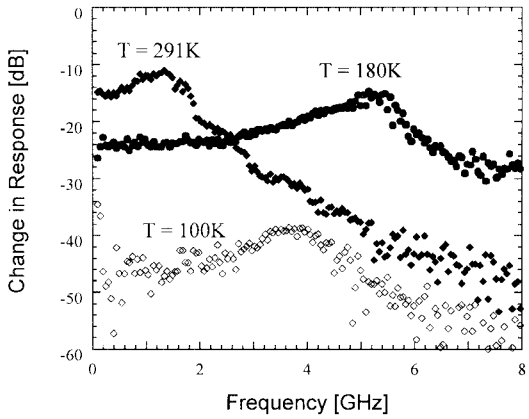

Fig. 8. Microwave modulation response at 100 K, 180 K, and room temperature (291 K). The dc injection current is 16 mA in all cases.

9 K, a sudden increase in slope efficiency is noticeable in Fig. 6 connected with a smaller increment of the threshold current. This might be attributed to a reduction of internal laser losses. Lasing is observed even at the lowest temperature investigated (7 K). Fig. 7 shows the CW threshold current versus temperature. Above 90 K, a wide temperature range with almost constant $I_{\rm th}(T)$ is measured. The minimum threshold current $I_{\rm th}$ of 9.4 mA is found at 180 K and a second minimum of 10.0 mA occurs at 120 K. Above 180 K, the threshold current increases toward the room-temperature value of 13.5 mA. These two $I_{\rm th}$ minima are common for all devices investigated. The physical reason for the second minimum is not yet understood. Due to self-heating, a shift of $T_{\rm opt}$ to lower stage temperatures is expected in CW operation. We can estimate a 35 K MQW temperature increase from 10 mA $\times$ 3.5 V heat power and 1000 K/W thermal resistance [8]. This temperature increase could generate a CW threshold minimum at the stage temperature of 145 K, but such a minimum is not observed.

In Fig. 8, we show the microwave modulation results between 100 K and room temperature. Below 100 K, the modulation response was hard to detect. A fixed dc injection current of 16 mA is chosen which is larger than the threshold current $I_{\rm th}(T)$ in that temperature range. The resonance frequency f_r increases from 1.4 GHz to a maximum of 5.2 GHz when the stage temperature is reduced from room temperature to 180 K. Since the injection current is kept constant at 16 mA, the bandwidth maximum at 180 K is attributed to the minimum threshold current (Fig. 7). Below 180 K, f_r decreases and the signal weakens considerably. At 100 K, we find $f_r = 3.8$ GHz. The weakening in output power is caused in part by the optical misalignment between the cryogenic VCL and the single-mode fiber outside the dewar window. The resonance frequency as a function of the injection current is given in Fig. 9. The modulation current efficiency η_m can be calculated from the slopes in Fig. 9 using (4). We find $\eta_m\ (180\ \mathrm{K}) = 3.1$ GHz/mA$^{1/2}$ and $\eta_m\ (291\ \mathrm{K}) = 1.4$ GHz/mA$^{1/2}$.

V. Discussion

For practical cryogenic applications, especially for parallel optical data links based on VCL arrays, the heat power generation is of great importance. A threshold voltage of about 3 V is typical for fused VCL's since the p-GaAs/p-InP interfaces causes a voltage drop due to charged defects. Our measured

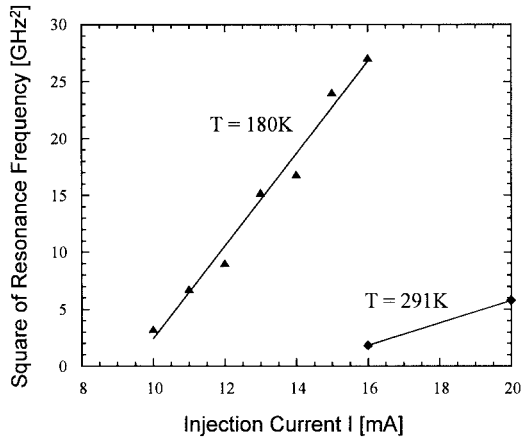

Fig. 9. Measured square of the resonance frequency versus injection current at $T = 180\,\mathrm{K}$ and at room temperature.

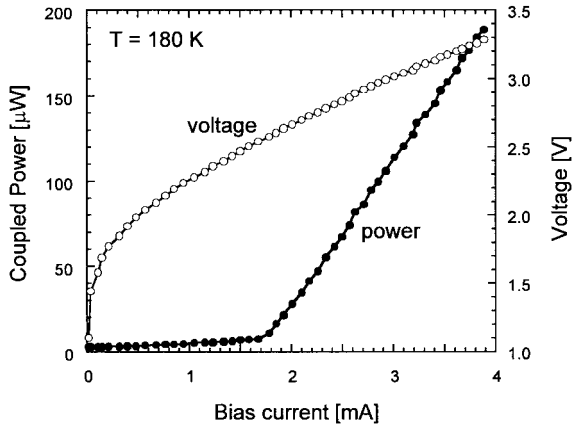

Fig. 10. Coupled optical power and device voltage versus pulsed current, measured at 180 K on a device without degradation. The wall-plug efficiency is about 1.5% at 4 mA bias current.

CW threshold current density is 8 kA/cm^2 assuming an oxide aperture diameter of 12 μm. This number is much larger than in previous devices that have shown values near 1 kA/cm^2 and threshold currents as low as 0.8 mA (3 μm aperture) [8]. Those record-low currents are correlated to an almost vanishing self-heating [8]. In our present devices, the high threshold currents may be caused by leakage currents due to packaging and low temperature degradation. The explanation is supported by the fact that a threshold current as low as 1.7 mA (180 K) is measured on a similar device. The pulsed L–I curve as well as the V–I characteristic of this device at the optimum temperature (180 K) are shown in Fig. 10. With a 2.5-V threshold voltage, the heat power is 4.25 mW at 180 K. Assuming 1000 K/W thermal resistance [8] we estimate only about 4 K MQW self-heating at threshold. For a 200-device array that we envision for future Terabits/s data links, the total heat power is about 0.9 W. This thermal budget would be acceptable with present cooling technology.

Compared to edge emitting lasers, the advantage of VCL's for high-speed operation is mainly due to the lower active volume [see (4)]. But VCL's also have the disadvantage of increasing gain offset resulting in lower differential gain (see Fig. 3). However, without any device optimization for

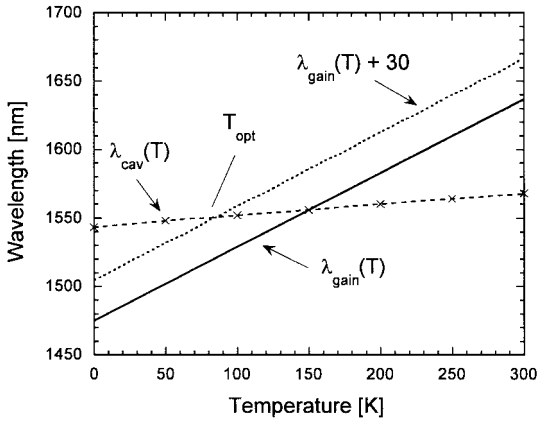

Fig. 11. Projected emission wavelength $\lambda_{\mathrm{cav}}(T)$ and gain peak wavelength $\lambda_{\mathrm{gain}}(T)$ for a device optimized for 80 K operation.

high-speed operation, our VCL exhibits a modulation current efficiency that can compete with results from a high-speed 1.5 μm edge emitting laser [5]. A clear improvement at lower temperatures is found with a maximum bandwidth at the optimum temperature ($T_{\mathrm{opt}} = 180\,\mathrm{K}$) that has a minimum threshold current. This indicates that the threshold current $I_{\mathrm{th}}(T)$ is the main influence on the temperature dependence of the bandwidth [see (4)]. With smaller active region diameters, larger efficiencies η_m are expected. With a 7-μm oxide aperture, $\eta_m = 2.76$ GHz/mA$^{1/2}$ has been measured on similar devices at room temperature [8].

With further improvements in device design and fabrication process we expect that cryogenic long-wavelength VCL's with 100 μA threshold current can be realized using small oxide apertures. Considering a target temperature of 80 K and an emission wavelength of about 1550 nm at that temperature, VCL design optimization is proposed as follows. Using (1)–(3), we show in Fig. 11 the required wavelength adjustment for achieving a minimum threshold current at 80 K. At 300 K, the MQW should exhibit a gain peak wavelength of 1637 nm with a VCL emission wavelength of 1568 nm. This emission wavelength can be obtained using thicker InP spacer layers. Variation of the MQW leads to the required shift of the gain spectrum. For example, with 7.5 nm thick $In_{0.76}Ga_{0.24}As_{0.86}P_{0.14}$ quantum wells (1.08% compressive strain) and $In_{0.71}Ga_{0.29}As_{0.51}P_{0.49}$ barriers (0.4% tensile strain), we calculate a room-temperature gain peak at 1640 nm. Other VCL improvements such as better lateral current confinement are expected to further reduce threshold current and self-heating.

The modulation bandwidth requires special attention in our device optimization to obtain high-speed operation at cryogenic temperatures. Nonuniform carrier distribution within the MQW is known to restrict the bandwidth [5]. The carrier distribution is affected by thermal carrier escape from the quantum wells, which depends on the energy barrier height as well as on the temperature. In our optimized design, the energy barrier is 113 meV for electrons, 244 meV for heavy holes, and 143 meV for light holes. In general, the chances for holes to escape from the quantum well are much smaller than for electrons, so that achieving a uniform hole distribution

is more difficult. Using tensile strained barriers reduces the energy barrier for light holes and thereby supports hole escape. Modulation measurements at very low temperatures are needed to show how effective our new MQW design is. It might be required to introduce an even lower hole barrier.

VI. Summary

CW lasing of double-fused 1.5 μm VCL's has been achieved at cryogenic temperatures as low as 7 K. The optimum operating temperature of our devices is 180 K corresponding to -30 nm gain offset from the emission wavelength. At that temperature, we measured a minimum threshold current as well as a maximum microwave modulation bandwidth. With further improvements in device design and fabrication process we expect that cryogenic long-wavelength VCL's with 100 μA threshold current can be realized using small oxide apertures.

Acknowledgment

The authors would like to thank V. Borzenets for his help on cryogenic testing setup.

References

[1] B. Lu, Y. C. Lu, J. Cheng, R. P. Schneider, J. C. Zolper, and G. Goncher, "Gigabit-per-second cryogenic optical link using optimized low-temperature AlGaAs-GaAs vertical-cavity surface-emitting lasers," *IEEE J. Quantum Electron.*, vol. 32, pp. 1347–1359, Aug. 1996.

[2] Y. A. Akulova, B. J. Thibeault, J. Ko, and L. A. Coldren, "Low-temperature optimized vertical-cavity lasers with submilliamp threshold currents over the 77–370K temperature range," *IEEE Photon. Technol. Lett.*, vol. 9, pp. 277–279, Mar. 1997.

[3] D. I. Babic, J. Piprek, K. Streubel, R. P. Mirin, N. M. Margalit, D. E. Mars, J. E. Bowers, and E. L. Hu, "Design and analysis of double-fused 1.55-μm vertical-cavity lasers," *IEEE J. Quantum. Electron.*, vol. 33, pp. 1369–1383, Aug. 1997.

[4] N. M. Margalit, K. A. Black, Y. J. Chiu, E. R. Hegblom, K. Streubel, P. Abraham, M. Anzlowar, J. E. Bowers, and E. L. Hu, "Top-emitting double-fused 1.5 μm vertical-cavity lasers," *Electron. Lett.*, vol. 34, pp. 285–287, Feb. 1998.

[5] R. Yu, R. Nagarajan, T. Reynolds, A. Holmers, J. E. Bowers, S. P. DenBaars, and C. E. Zah, "Ultrahigh speed performance of a quantum well laser at cryogenic temperatures," *Appl. Phys. Lett.*, vol. 65, pp. 528–530, Aug. 1994.

[6] J. Piprek, Y. Akulova, D. I. Babic, L. A. Coldren, and J. E. Bowers, "Minimum temperature sensitivity of 1.55 μm vertical-cavity lasers at -30nm gain-offset," *Appl. Phys. Lett.*, vol. 72, pp. 1814–1816, Apr. 1998.

[7] S. Rapp, J. Piprek, K. Streubel, J. Andre, and J. Wallin, "Temperature sensitivity of 1.54 μm vertical cavity lasers with an InP-based Bragg reflector," *IEEE J. Quantum Electron.*, vol. 33, pp. 1839–1845, Oct. 1997.

[8] N. M. Margalit, J. Piprek, S. Zhang, D. I. Babic, K. Streubel, R. P. Marin, J. R. Wesselmann, J. E. Bowers, and E. L. Hu, "64°C continuous-wave operation of 1.5 μm vertical-cavity laser," *IEEE J. Select. Topics Quantum Electron.*, vol. 3, pp. 359–365, Apr. 1997.

Y. M. Zhang, photograph and biography not available at the time of publication.

J. Piprek (M'94–SM'98), photograph and biography not available at the time of publication.

N. Margalit, photograph and biography not available at the time of publication.

M. Anzlowar, photograph and biography not available at the time of publication.

J. Bowers (S'78–M'81–SM'85–F'93), photograph and biography not available at the time of publication.